LAWRENCE
LIVERMORE
NATIONAL
LABORATORY

UCRL-JRNL-221627

Influence of Black Annealing Oxide Scale on the Anodic Behavior of Alloy 22

Raul B. Rebak, Robert A. Etien, Steve R. Gordon, Gabriel O. Ilevbare

May 25, 2006

Corrosion

Disclaimer

INFLUENCE OF BLACK ANNEALING OXIDE SCALE ON THE ANODIC BEHAVIOR OF ALLOY 22

Raul B. Rebak, Robert A. Etien, Steve R. Gordon and Gabriel O. Ilevbare
Lawrence Livermore National Laboratory
7000 East Ave, L-631
Livermore, CA 94550, USA

ABSTRACT

The resistance of Alloy 22 (N06022) to localized corrosion, mainly crevice corrosion, has been extensively investigated in the last few years. The effect of influencing variables such as temperature, applied potential, chloride concentration and nitrate inhibitor concentration have been addressed previously. At this time, it was important to address the effect an oxide film or scale that forms during the high temperature annealing process or solution heat treatment (SHT) and its subsequent water quenching. Electrochemical tests such as cyclic potentiodynamic polarization (CPP) have been carried out to determine the repassivation potential for localized corrosion and to assess the mode of attack on the specimens. Tests have been carried out in parallel using mill annealed (MA) specimens free from oxide on the surface. The comparative testing was carried out in six different electrolyte solutions at temperatures ranging from 60°C to 100°C. Results show that the repassivation potential of the specimens containing the black anneal oxide film on the surface was practically the same or higher as the repassivation potential for oxide-free specimens.

Keywords: N06022, Black Annealing, Solution Heat Treatment, Chloride, Temperature, Corrosion Rate, Crevice Corrosion, Repassivation Potential

INTRODUCTION

Alloy 22 (N06022) is nickel (Ni) based and contains nominally 22% chromium (Cr), 13% molybdenum (Mo) and 3% tungsten (W). [1] Alloy 22 belongs to the Ni-Cr-Mo family of nickel based alloys, which also include alloys such as C-4 (N06455), C-276 (N10276), C-2000 (N06200), 59 (N06059) and 686 (N06686). [1] The Ni-Cr-Mo alloys were designed to withstand the most aggressive industrial applications, including reducing acids such as hydrochloric and oxidizing acids such as nitric. Chromium is the beneficial alloying element added for protection against oxidizing conditions and molybdenum is the beneficial alloying element to protect against reducing conditions. [2-4] The base element (nickel) protects the alloy against caustic conditions. [2-4] All three elements, Ni, Cr and Mo act synergistically to provide

resistance to environmentally assisted cracking in hot concentrated chloride solutions. [2-4] The alloying elements Cr and Mo also provide resistance to localized corrosion such as pitting and crevice corrosion in chloride containing solutions. Some of the Ni-Cr-Mo alloys also contain a small amount of tungsten (W), which may act in a similar way as Mo regarding protection against localized corrosion. [5] Ni-Cr-Mo alloys are practically immune to pitting corrosion but they may suffer crevice corrosion under aggressive environmental conditions. The presence of oxyanions in the electrolyte inhibits crevice corrosion. [6-8] These oxyanions include mainly nitrate, sulfate and carbonate. [8-9] Fluoride ions also may inhibit crevice corrosion in Alloy 22. [10] A minimum ratio of inhibitor to chloride is needed for the inhibition to occur. [6-10]

Due to its excellent resistance to all forms of corrosion, Alloy 22 (N06022) has been selected to fabricate the external shell of the Yucca Mountain high-level nuclear waste containers. [11] The fabrication of the containers involves the rolling of plates into shape and then producing circumferential and longitudinal welds. Before inserting the nuclear waste into the container, these will be fully solution annealed to homogenize the microstructure and composition of the weld seams and to relieve residual stresses that might have been introduced during welding. [11] The method of solution annealing or solution heat treatment (SHT) will be in an uncontrolled atmosphere (in air). This is generally called black annealing since a black (and greenish) oxide scale grows on the exposed surfaces of the material. The purpose of this solution annealing is not to form the oxide scale but to change the microstructure of the weld and to relieve the stresses. The oxide scale formation on the surface is a consequence of the treatment, not the desired effect. After heating at temperature for the specified time, the containers will be cooled down rapidly using water (water quenching). [11] The rapid cooling is necessary to avoid the precipitation of detrimental second phases in Alloy 22.

It has been shown that the corrosion rate of black annealed creviced specimens decreased with time when it was exposed to aerated chloride and nitrate containing solutions at 100°C. [12] Even though the corrosion rate of black annealed specimens was slightly more erratic than that of freshly polished specimens, the corrosion rates of both types of specimens were in the order of only 50 nm/year after 100 days exposure. [12] It was of interest to investigate the influence of the black annealed oxide film for its resistance to crevice corrosion as compared to freshly polished specimens. The current work shows results comparing the repassivation potential of freshly polished creviced Alloy 22 specimens and specimens that were SHT in air at 2050°F (1121°C) for 20 min. and then water quenched. The SHT specimens were non-welded specimens since the objective was to separate the effect of the black oxide scale from the possible change in the microstructure of the weld during the high temperature treatment. Both pure chloride solutions and mixed anion solutions were used. Pure chloride solutions do not represent environmental conditions at the Yucca Mountain repository. [11]

EXPERIMENTAL

The specimens were machined from 1.25-inch thick plates (~32 mm). Table 1 shows the chemical composition of the material. The specimens were in the form of multiple crevice assemblies (MCA) or lollipops (Figure 1). The specimens were named starting with the letters DEA or JE and followed by a consecutive number. These designations are arbitrary. The dimensions of the MCA were approximately 2 mm thick and a minimum of 11 cm long. The test part of the specimen was an annulus of 20 mm outside diameter and 7 mm inside diameter. The exposed surface area of each specimen was 7.43 cm². This surface area included the area covered by the crevice formers, which was approximately 1.5 cm². The crevice formers (CF) were mounted on both sides of the specimen (Figure 1). Each crevice former consisted of a washer made of a ceramic material (alumina) containing 12 crevicing spots or teeth with gaps in between the teeth (ASTM G 48). [13] Before mounting them onto the metallic specimens, the CF were covered with PTFE tape to ensure a tight crevicing gap. [14-16] The specimens had a ground finish of 600

grit paper. There are two types of specimens mentioned in this work: (1) The as-received wrought mill annealed (MA) and (2) the solution heat-treated (MA + SHT) which were annealed in air for 20 min at 1121°C and then water quenched. The latter specimens were finished with 600-grit paper before the heat treatment but the final black oxide film (BOF) formed as a consequence of solution annealing and water quenching was not disturbed prior to testing. The SHT specimens were black with slight tones of green, typical of high temperature formed chromium oxide. The SHT process that the specimens suffered for the current testing was carried out in an attempt to simulate the actual intended annealing conditions of the containers. It is planned to heat the containers in air up to 1121 ± 28°C, and soak them at this temperature for a minimum time of 20 min. and then quench the containers at a rate of 83°C/min to a temperature below 370°C.

The characteristics of the solution-annealed oxide have been described in a separated study. [17] The thickness of the oxide was 1 μm and higher and contained an internal layer of Cr_2O_3 and an external layer of mixed Cr, Ni and Fe oxide. Molybdenum was not found in the oxide. [17] The studied specimens were all wrought non-welded specimens, also called base metal. During the SHT process of 1121°C for 20 min. the base microstructure of Alloy 22 does not change. That is, there is no grain growth or changes in microstructure of the metal. [18]

For the electrochemical testing, the MCA specimens were partially immersed, that is, the water line crossed the stem of the specimen (Figure 1).

Table 2 shows the composition of the six test solutions. The compositions are given in molar (M) and molal (*m*). Molar is moles of the salt per liter of solution and molal is moles of the salt per kilogram of solvent (water). Nitrogen (N_2) was purged through the solution at a flow rate of 100cc/min for 24 hours while the corrosion potential (E_{corr}) was monitored. Nitrogen bubbling was continued throughout all the electrochemical tests. The electrochemical tests were conducted in a one-liter, three-electrode, borosilicate glass flask (ASTM G 5). [13] A water-cooled condenser combined with a water trap was used to avoid evaporation of the solution and to prevent the ingress of air (oxygen). The temperature of the solution was controlled using a heating mantle connected to a temperature control device. All the tests were carried out at ambient pressure. The reference electrode was saturated silver chloride (SSC) electrode, which has a potential 199 mV more positive than the standard hydrogen electrode (SHE). The reference electrode was connected to the solution through a water-jacketed Luggin probe so that the electrode was maintained at near ambient temperature. The counter electrode was a flag (40 cm^2) of platinum foil spot-welded to a platinum wire. All the potentials in this paper are reported in the SSC scale.

The test sequence for each specimen consisted of three parts: (1) E_{corr} evolution as a function of time for 24 h, (2) Polarization Resistance (ASTM G 59) [13] three consecutive times and (3) Cyclic Potentiodynamic Polarization (CPP) (ASTM G 61). [13]

Polarization Resistance (ASTM G 59): Corrosion rates (CR) were obtained using the polarization resistance method (ASTM G 59). Each one of these tests lasts approximately four minutes. An initial potential of 20 mV below the corrosion potential (E_{corr}) was ramped to a final potential of 20 mV above E_{corr} at a rate of 0.167 mV/s. Linear fits were constrained to the potential range of 10 mV below E_{corr} to 10 mV above E_{corr} putting the potential (independent variable) in the X-axis. The linear fit produces a value of slope, which is the resistance to polarization R_p. The Tafel constants, b_a and b_c, were assumed to be ± 0.12 V/decade. Corrosion rates were calculated using Equation 1

$$i_{corr} = \frac{1}{R_p} \cdot \frac{b_a \cdot b_c}{2.303(b_a + b_c)} \ldots and \cdots CR(\mu m / yr) = k \frac{i_{corr}}{\rho} EW \qquad \textbf{(1)}$$

Where k is a conversion factor, i_{corr} is the calculated corrosion current density in A/cm^2 (using values of the slope R_p in Ohm-cm^2), EW is the equivalent weight (dimensionless), and ρ is the density of Alloy

22 (8.69 g/cm^3). Assuming an equivalent dissolution of the major alloying elements as Ni^{2+}, Cr^{3+}, Mo^{6+}, Fe^{2+}, and W^{6+}, the EW for Alloy 22 is 23.28 (ASTM G 102). [13]

Cyclic Potentiodynamic Polarization - CPP (ASTM G 61): The cyclic potentiodynamic polarization technique, CPP (ASTM G 61) [13] is one of the tests commonly used to assess the susceptibility of Alloy 22 to localized corrosion and its passive stability. The potential scan was started 150 mV below E_{corr} at a set scan rate of 0.167 mV/s. The scan direction was reversed when the current density reached 5 mA/cm^2 in the forward scan. Depending on the range of applied potentials, each CPP test could last between 1 h and 3 h. After the CPP tests, the specimens were examined in an optical stereomicroscope at a magnification of at least 20 times to establish the mode and location of the attack.

RESULTS AND DISCUSSION

The Corrosion Potential (E_{corr}) and the Corrosion Rate (CR)

Tables 3-5 show the values of the corrosion potential (E_{corr}) and the corrosion rate (CR) of MA and SHT specimens after 24-h immersion in the deaerated electrolytes. The values of E_{corr} and CR in Tables 3-5 are for comparative purposes only and do not represent steady-state values. That is, the values of E_{corr} and CR in Tables 3-5 are not the values at which Alloy 22 would ultimately corrode when exposed to similar environments in aerated conditions for exposure times longer than 24-h. In general, Tables 3-5 show that the E_{corr} of the MA specimens was lower than that of the SHT specimens. This suggests that the high temperature air formed oxide film (SHT) provided some protection in the respective electrolyte solutions during the early immersion times. Figure 2 and Table 3 show the 24-h corrosion rates for Alloy 22 in deaerated 5 M $CaCl_2$ solution at 60°C and 90°C. For both types of specimens the corrosion rate in 5 M $CaCl_2$ was slightly higher for the higher temperature. It is also apparent that in this electrolyte the corrosion rate of the SHT specimens was lower than that of the MA specimens, again suggesting that the high temperature air formed oxide film provided early protection against corrosion in these environments. Figure 3 shows the 24-h corrosion rates for Alloy 22 in deaerated 6 m NaCl + 0.9 m KNO_3 solution at 80°C and 100°C. Again, similarly as in 5 M $CaCl_2$ (Figure 2) it is apparent that the corrosion rate of the SHT specimens was lower than that of the MA specimens, also suggesting that the high temperature air formed oxide film provided early protection against corrosion in these nitrated environments. The remaining CR data in Tables 3-5 show in general a similar behavior (with higher data scattering), that is, the corrosion rate of the SHT specimens was lower than that of the MA specimens. Most of the corrosion rates in Tables 3-5 are between 0.1 μm/year and 1 μm/year. It is expected that the corrosion rate of Alloy 22 will decrease as the exposure time in the electrolytes increases. [12,19-20] It is also expected that the E_{corr} values in Tables 3-5 will increase as a function of time. The rate of increase and the final steady-state value will depend on the composition, pH and temperature of the electrolyte. The presence of oxygen in the electrolyte will also affect the rate of increase of E_{corr}.

Cyclic Potentiodynamic Polarization (CPP)

Figure 4 shows the cyclic potentiodynamic polarization curves for individual Alloy 22 specimens in deaerated 5 M $CaCl_2$ solutions at 60°C. Figure 4 shows that the polarization curve of the SHT specimen was different than the polarization curve for the MA polished specimen. Basically, the MA specimen can be polarized to higher potentials and the curve does not show hysteresis during the reverse scan. It is apparent that the SHT specimen can produce more output current for the same initial applied potential up to 200 mV SSC than the MA polished specimen. It is likely that the oxide scale in the SHT specimen reacts with the electrolyte providing the additional current. After the CPP tests, the SHT specimens showed attack on the bold surfaces of the specimen, while the MA polished specimen

showed minimal dull crevice corrosion[9] even though the latter was polarized to 1 V or 800 mV higher higher than the SHT specimens (Table 6). Figure 4 also shows that corrosion potential for the SHT specimen was higher than for the MA specimen and that the passive current density for the SHT specimen was slightly lower than for the MA polished specimen. [21] This seems to confirm the corrosion rate findings discussed in the previous section. Again, these are observations based on short-term tests. The presence of the anodic peak in the middle region of the MA specimen in Figure 4 has been discussed before. [22] It has been explained that a partial breakdown and then subsequent repassivation occurs at the potential of the anodic peak. [22]

Figure 5 shows the CPP curves for both types of specimens in 5 M $CaCl_2$ at 90°C. While the passive current density for the SHT specimen was lower than for the MA specimen, their breakdown potential and repassivation potentials were similar. Table 6 shows that the mode of attack after the CPP was different for these two types of specimens.

Figure 6 shows the CPP curves for both types of specimens in 6 m NaCl + 0.9 m KNO_3 solution at 100°C. Even though the SHT specimen had an initially higher corrosion potential, the full anodic behavior and the repassivation potential for both types of specimens were similar. Both curves show a hysteresis in the reverse scan suggesting the presence of localized corrosion. Table 6 shows that both types of specimens suffered crystallographic crevice corrosion.

Parameters from the Anodic Polarization Curves

In CPP curves (e.g. Figures 4-6) there are several typical potentials. They can be divided in two groups: (1) Breakdown potentials in the forward scan, called E20 and E200 that represent the potential that needs to be applied to the specimen in the forward scan for the current density to reach respectively 20 μA/cm² and 200 μA/cm². (2) Repassivation potentials in the reverse scan, called ER10, ER1 and ERCO. ER10 and ER1 represent the potential that needs to be applied in the reverse scan for the current density to reach 10 μA/cm² and 1 μA/cm², respectively. ERCO represents the potential at which the reverse scan crosses over (CO) the forward scan in the passive region of potentials. [8,9,16,23-25] That is, in the forward scan, when the current density reaches for example 200 μA/cm² it can be considered that the alloy has lost its passive mode and that when the current density in the reverse scan has reaches 1 μA/cm², the alloy has regained its passive behavior prior to the breakdown. Tables 3-5 list these parameters for both types of specimens in the six investigated electrolytes. Tables 3-5 show that the value of ER1 to indicate repassivation is always available from a CPP curve; however ERCO values only exist when the intersection occurs, that is, in presence of an obvious hysteresis.

Figure 7 shows the parameters from the CPP (Data from Table 3) for the tests carried out in 1 M NaCl solution at 90°C. The 24-h E_{corr} values are also shown. Figure 7 shows that the anodic behavior of Alloy 22 was practically the same for both types of specimens. The average E_{corr} for the SHT specimens was slightly higher than for the MA specimens. The breakdown potentials (E20 and E200) were practically identical for SHT and MA specimens. The repassivation potentials (ER10, ER1 and ERCO) of the SHT specimens were slightly higher than those of the MA specimens. It is possible that the presence of the air formed oxide in the SHT specimens provided a wider gap with the crevice formers and allowed for a faster repassivation during the reverse scan in the CPP tests. Table 6 shows that both type of specimens suffered crystallographic crevice corrosion in 1 M NaCl at 90°C after the CPP tests. Figure 8 shows the average breakdown potential E20 for pure chloride solutions both at 60°C and at 90°C (data in Table 3). In 1 M NaCl and 5 M $CaCl_2$ solutions at 60°C, E20 was lower for the SHT than for the MA specimens (Figure 8). [21] At 90°C, the E20 in 1 M NaCl was the same for MA and SHT specimens but the E20 in 5 M $CaCl_2$ was lower for the MA specimens. Figure 9 shows the average repassivation potential ER1 in the pure chloride solutions (data in Table 3). Similarly as for the breakdown potential E20

(Figure 8), the ER1 was higher for the MA specimens in the less aggressive electrolytes (60°C) and higher for the SHT specimens in the more aggressive electrolytes (90°C).

Table 4 shows the breakdown potentials (E20) and the repassivation potentials (ER1) for the specimens tested in solutions containing 6 m NaCl plus two different amounts of KNO_3, both at 80°C and 100°C.. Figure 10 shows the average E20 for both types of specimens in at the two tested temperatures in the two tested electrolytes. In general, there was little effect of the presence of the black anneal oxide film on the E20 in the tested conditions. Figure 11 shows the ER1 for the same conditions as in Figure 10. In both solutions and at both temperatures, ER1 for the SHT specimens was higher than for the MA specimens, suggesting a higher resistance to localized corrosion for the specimens with the black oxide film. This difference was especially important in the solution containing the lowest amount of nitrate (0.3 m) at the higher temperature (100°C). Table 6 shows that the mode of attack of both types of specimens was similar in each tested conditions. At the lower temperature (80°C) and at the higher nitrate concentration (0.9 m), the attack in the SHT specimen seemed slightly more pronounced than in the MA specimens. This is mainly due to a larger amount of crevice corrosion and pitting-like corrosion in the bold surfaces.

Figures 12 and 13 show the average breakdown and repassivation potentials (E20 and ER1) for the specimens tested in 3.5 m NaCl + 0.525 m KNO_3 at 60°C and 100°C and in 0.1 m NaCl + 0.001 m $NaHCO_3$ at 60°C and 95°C (data are in Table 5). In general, the E20 was slightly higher for the SHT specimens in each of the higher temperature solutions (95°C and 100°C) (Figure 12). Figure 13 shows that the ER1 was lower for SHT specimens in the NaCl + KNO_3 solution at both temperatures. On the other hand, in the dilute NaCl + $NaHCO_3$ solution the ER1 was always higher for the SHT specimens. Data in Figures 12-13 and in Table 5 in general confirm that the SHT specimens seem more resistant to localized corrosion in the more aggressive electrolytes.

Figure 14 shows the repassivation potentials ER1 for two chloride concentrations and for fixed ratio of nitrate to chloride ratio at 100°C. At the lower chloride concentration the repassivation potential of the SHT specimens was slightly lower than for the MA specimens, but this trend was reversed at the higher chloride concentration. The data in Figure 14 may suggest that for the rate nitrate over chloride ratio of 0.15, the higher base chloride concentration of 6 m is more aggressive.

Type of Attack in the Specimens after Anodic Polarization

Table 6 shows a description of the attack in the specimens after the CPP tests. In general, for both SHT and MA specimens, the mode of attack was the same, especially in the most aggressive conditions such as at the higher temperatures and lower nitrate to chloride ratios. For example in the 1 M NaCl solution at 90°C, the main mode of attack was crystallographic crevice corrosion for both types of specimens (Figures 15 and 16). Similarly in the 6 m NaCl + 0.3 m KNO_3 at 100°C, the main mode of attack for both types of specimens was also crevice corrosion (Figures 17 and 18). In 5 m $CaCl_2$ at 90°C, the attack started at the edge of the crevice formers but propagated towards outside the crevice formers, on the flat face of the specimen for the MA condition and on the edge and borders for the SHT specimens (Figures 19 and 20). In the less aggressive environments (lower temperatures and higher nitrate to chloride ratio) the mode of attack was slightly different for both types of specimens. In the pure chloride solutions (1 M NaCl and 5 M $CaCl_2$) at 60°C the attack in the MA specimens was mostly transpassivity and dull crevice corrosion. (For description of types of attack, e.g. dull vs. crystalline see Ref. 9) However, for the SHT specimens, the main attack was boldly pitting corrosion type of attack. Similarly for the 6 m NaCl + 0.9 m KNO_3 at 80°C, the attack in the MA specimens was transpassivity and dull crevice corrosion while in the SHT specimens the attack was crystallographic crevice corrosion and pitting

like in the bold areas. Figures 21 and 22 show the mode of attack in 0.1 m NaCl + 0.001 m $NaHCO_3$ solution at 95°C for MA and SHT specimen respectively. For the MA specimen the attack was uniform mostly dull crevice corrosion around the rim of the crevice former. For the SHT specimen the attack is partly crystallographic crevice corrosion and partly edge and border attack. In 0.1 m NaCl + 0.001 m $NaHCO_3$ solution at 60°C (Figures 23 and 24) the attack in the MA specimen was mostly transpassivity and in the SHT specimen border attack.

Concluding Remarks

Cyclic polarization curves have been carried out to determine the effect of the solution heat-treated (SHT) high temperature oxide scale on the resistance of Alloy 22 to localized corrosion. To assess the effect of the black oxide film tests were performed in parallel using mill annealed (MA) specimens which were freshly polished to provide a more or less oxide free surface. Both type of specimens (SHT and MA) had the same non-welded wrought crystalline microstructure. The basic difference was the presence of the high-temperature air formed oxide in the SHT specimens. The tests were carried out in a variety of environments from pure chloride solutions (such as 5 M $CaCl_2$) to solutions that contained chloride plus the inhibitive nitrate oxyanion (such as 6 m NaCl + 0.9 m KNO_3). Tests were also carried out in dilute solutions such as 0.1 m NaCl + 0.001 m $NaHCO_3$. The test solutions had a range of pH from 4.7 to 8. The test temperature ranged from 60°C to 100°C. In most of the tested conditions, the SHT specimens had the same repassivation potential as the MA specimens or were slightly higher than for the MA specimens. In a few cases, especially at the lower tested temperatures the repassivation potentials for the SHT specimens were lower than for the MA specimens. A higher repassivation potential indicates a higher resistance to localized corrosion. That is, the repassivation potential seems to be dependent on the tested electrolyte. The mode of attack of the MA and SHT materials was also similar. In cases of low environmental aggressiveness the mode of attack varied slightly between MA and SHT specimens; however the metrics (repassivation potential values) remained practically the same.

Under the tested conditions the black annealing oxide scale does not seem to have a detrimental effect on the resistance of Alloy 22 to localized corrosion.

CONCLUSIONS

1. The short-term (24-h) E_{corr} of Alloy 22 in deaerated solutions was generally higher for the SHT specimens than for the MA specimens.

2. The short-term corrosion rate in deaerated electrolytes was generally lower for the SHT than for the MA specimens.

3. The repassivation potentials ER1 for the SHT specimens were comparable to the MA specimens. In the most aggressive electrolytes the ER1 of the SHT specimens was slightly higher than for the MA specimens. In the less aggressive electrolytes the ER1 for the MA specimens was slightly higher.

4. The mode of localized corrosion attack of the SHT and MA was practically the same. When the tested conditions were less aggressive (for example at the lower temperatures) the mode of attack of the two types of specimens varied slightly.

ACKNOWLEDGMENTS

This work was performed under the auspices of the U. S. Department of Energy (DOE) by the University of California Lawrence Livermore National Laboratory under contract N° W-7405-Eng-48. This work is supported by the Yucca Mountain Project, which is part of the Office of Civilian Radioactive Waste Management (OCRWM)

DISCLAIMER

REFERENCES

1. ASTM International, Annual Book of ASTM Standards, Volume 02.04 "Non-Ferrous Metals" Standard 575 B (West Conshohocken, PA: ASTM International, 2002)
2. R. B. Rebak and P. Crook, Transportation, Storage and Disposal of Radioactive Materials, PVP-Vol. 483, p. 131 (American Society of Mechanical Engineers, 2004: New York, NY)
3. R. B. Rebak in Corrosion and Environmental Degradation, Volume II, p. 69 (Wiley-VCH, 2000: Weinheim, Germany)
4. R. B. Rebak and P. Crook, *Advanced Materials and Processes*, February 2000
5. R. B. Rebak and P. Crook, Proceeding of the Symposium Critical Factors in Localized Corrosion III, PV 98-17, p. 289 (The Electrochemical Society, 1998: Pennington, NJ)
6. G. A. Cragnolino, D. S. Dunn and Y.-M. Pan "Localized Corrosion Susceptibility of Alloy 22 as a Waste Package Container Material," Scientific Basis for Nuclear Waste Management XXV, Vol. 713, p. 53 (Materials Research Society 2002: Warrendale, PA)
7. D. S. Dunn, L. Yang, C. Wu and G. A. Cragnolino, Mat. Res. Soc. Symp. Proc. Vol 824 (MRS, 2004: Warrendale, PA)
8. J. H. Lee, T. Summers and R. B. Rebak, Paper 04692, Corrosion/2004 (NACE International, 2004: Houston, TX)
9. R. B. Rebak, Paper 05610, Corrosion/2005 (NACE International, 2005: Houston, TX)
10. R. M. Carranza, M. A. Rodríguez and R. B. Rebak, "Inhibition of Chloride Induced Crevice Corrosion in Alloy 22 by Fluoride Ions," Paper 06626, Corrosion/2006 (NACE International, 2006: Houston, TX)
11. G. M. Gordon, Corrosion, 58, 811 (2002)
12. K. J. King, J. C. Estill, G. A. Hust, M. L. Stuart and R. B. Rebak, Paper 05607, Corrosion/2005 (NACE International, 2005: Houston, TX)
13. ASTM International, Annual Book of ASTM Standards, Volume 03.02 "Wear and Erosion; Metal Corrosion" G-15, G-61, etc. (West Conshohocken, PA: ASTM International, 2004)
14. K. J. Evans, S. D. Day, G. O. Ilevbare, M. T. Whalen, K. J. King, G. A. Hust, L. L. Wong, J. C. Estill and R. B. Rebak, Transportation, Storage and Disposal of Radioactive Materials, PVP-Vol. 467, p. 55 (American Society of Mechanical Engineers, 2003: New York, NY)
15. G. O. Ilevbare, K. J. King, S. R. Gordon, H. A. Elayat, G. E. Gdowski and T. S. E. Gdowski, Journal of The Electrochemical Society, 152, 12, B547-B554, 2005
16. B. A. Kehler, G. O. Ilevbare and J. C. Scully, Corrosion, p. 1042 (2001)
17. C.A. Orme, Internal Report from Lawrence Livermore National Laboratory (April 2003).
18. B. S. El-Dasher, T. S. Edgecumbe and S. G. Torres, Metall. And Mater. Trans. A, **37A**, 1027 (2006).
19. K. J. Evans and R. B. Rebak in Corrosion Science – A Retrospective and Current Status in Honor of Robert P. Frankenthal, PV 2002-13, p. 344-354 (The Electrochemical Society, 2002: Pennington, NJ).
20. R. M. Carranza, M. A. Rodríguez and R. B. Rebak, "Passivity of Alloy 22 in Chloride and Fluoride Containing Solutions," Paper 06-02, 16th International Corrosion Congress, Beijing, China 19-24 September 2005.
21. R. A. Etien, S. R. Gordon and G. O. Ilevbare, Paper PVP2005-71652, from proceedings of the Pressure Vessels and Piping Division Conference, 17-21 July 2005, Denver, CO.
22. G. O. Ilevbare, Paper PVP2002-1614, PVP-Vol. 449, from proceedings of the Pressure Vessels and Piping Division Conference, 05-09 August 2002, Vancouver, BC, pages 55-65 (ASME, 2002: New York, NY).
23. K. J. Evans, A. Yilmaz, S. D. Day, L. L. Wong, J. C. Estill and R. B. Rebak "Comparison of Electrochemical Methods to Determine Crevice Corrosion Repassivation Potential of Alloy 22 in Chloride Solutions," JOM, January 2005 (TMS, 2005: Warrendale, PA)
24. D. S. Dunn and C. S. Brossia, Paper 02548, Corrosion 2002 (NACE International, 2002: Houston, TX)
25. K. J. Evans, L. L. Wong and R. B. Rebak, Transportation, Storage and Disposal of Radioactive Materials, PVP-Vol. 483, p. 137 (American Society of Mechanical Engineers, 2004: New York, NY)

TABLE 1 -
CHEMICAL COMPOSITION IN WEIGHT % OF THE TESTED MCA SPECIMENS
ALL SPECIMENS WROUGHT MILL ANNEALED

Specimens/Element	**Ni**	**Cr**	**Mo**	**W**	**Fe**	**Others**
Nominal ASTM B 575 N06022	50-62	20-22.5	12.5-14.5	2.5-3.5	2-6	2.5Co-0.5Mn-0.35V (A)
DEA Specimens Heat 2277-1-3265	~57	21.2	12.9	2.5-3.5	3.9	0.7Co-0.25Mn-0.17V
JE Specimens Heat 059902LL1	59.56	20.38	13.82	2.64	2.85	0.17V-0.16Mn

(A) Maximum

TABLE 2 - TEST SOLUTIONS

Test Solution	$[NO_3^-]/[Cl^-]$	Ambient pH	Test Temperature (°C)
1 M NaCl	0	6.1	60, 90
5 M $CaCl_2$	0	4.7	60, 90
6 m NaCl + 0.9 m KNO_3	0.15	6.2	80, 100
6 m NaCl + 0.3 m KNO_3	0.05	6.3	80, 100
3.5 m NaCl + 0.525 m KNO_3	0.15	6.7	60, 100
0.1 m NaCl + 0.001 m $NaHCO_3$	0.01 *	8.0	60, 95
	* $[HCO_3^-]/[Cl^-]$		

TABLE 3
CHARACTERISTIC POTENTIALS (mV, SSC) AND CORROSION RATES FOR ALLOY 22

Specimen ID	Type of Specimen	E_{corr}, 24 h (mV, SSC)	Corrosion Rates (μm/year) after 24-h	E20 (mV, SSC)	E200 (mV, SSC)	ER10 (mV, SSC)	ER1 (mV, SSC)	ERCO (mV, SSC)
5 M $CaCl_2$, 60°C, pH 4.7								
DEA3375	MA 600	-267	0.2469, 0.5714	(2 AP) 876	978	837	694	None (80 AP)
DEA3387	MA 600	-360	2.111, 1.123, 3.055	(-63 AP) 897	1000	861	728	None
DEA3369	SHT	-278	0.1361, 0.1551, 0.1443	61	105	-43	-115	-163
DEA3368	SHT	-194	0.0993, 0.0793, 0.1016	84	126	-40	-111	-164
5 M $CaCl_2$, 90°C, pH 4.7								
DEA3376	MA 600	-319	1.3430, 0.8258, 0.9245	-22	78	-163	-185	-183
DEA3388	MA 600	-354	3.4470, 3.6540, 3.2220	-130	76	-123	-180	-35
DEA3370	SHT	-309	0.2334, 0.2282, 0.2469	25	50	-99	-156	-200
DEA3371	SHT	-189	0.5906, 0.5273, 0.5534	27	51	-111	-165	-185
1 M NaCl, 60°C, pH 6.1								
JE3321	MA 600	-456	0.244, 0.279, 0.317	723	797	628	163	84 MH
JE3322	MA 600	-579	1.633, 1.045, 1.157	697	819	668	65	28
JE3301	SHT	-387	0.286, 0.276, 0.303	479	935	185	17	-10
JE3302	SHT	-390	0.267, 0.279, 0.274	317	908	140	-4	77
1 M NaCl, 90°C, pH 6.1								
JE3324	MA 600	-593	2.413, 2.117, 2.300	261	438	-38	-117	-126
JE3328	MA 600	-484	0.422, 0.438, 0.443	228	475	-33	-113	-109
JE3303	SHT	-254	0.257, 0.251, 0.244	307	448	94	-39	-80
JE3304	SHT	-412	0.268, 0.277, 0.282	179	422	78	-13	66
MA 600 = As received wrought specimens finished with paper 600 (polished), SHT = Solution heat-treated specimens containing the black annealed oxide film (BOF) on the surface (1121°C for 20 min plus water quenched). MH = Minor or no hysteresis								

TABLE 4
CHARACTERISTIC POTENTIALS (mV, SSC) AND CORROSION RATES FOR ALLOY 22

Specimen ID	Type of Specimen	E_{corr}, 24 h (mV, SSC)	Corrosion Rates (μm/year) After 24-h	E20 (mV, SSC)	E200 (mV, SSC)	ER10 (mV, SSC)	ER1 (mV, SSC)	ERCO (mV, SSC)
6 m NaCl + 0.9 m KNO_3, 80°C (NO_3^-/Cl^- = 0.15), pH 6.2								
JE3317	MA 600	-501	0.301, 0.279, 0.256	637	810	635	9	-52
JE3318	MA 600	-471	0.304, 0.235, 0.398	649	800	624	-8	-27
JE3309	SHT	-371	0.0803, 0.0804, 0.0816	769	909	101	-6	-12
JE3310	SHT	-257	0.158, 0.160, 0.160	756	917	134	13	-25
6 m NaCl + 0.9 m KNO_3, 100°C (NO_3^-/Cl^- = 0.15) , pH 6.2								
JE3319	MA 600	-460	0.558, 0.301, 0.308	430	737	-6	-77	-84
JE3320	MA 600	-486	3.663, 3.841, 3.643	527	777	-8	-82	-88
JE3311	SHT	-303	0.411, 0.341, 0.380	362	843	16	-15	-11
JE3312	SHT	-316	0.274, 0.274, 0.258	480	863	14	-41	-48
6 m NaCl + 0.3 m KNO_3, 80°C (NO_3^-/Cl^- = 0.05) , pH 6.3								
JE3313	MA 600	-515	0.3815, 0.5266, 0.3599	437	832	-20	-103	-114
JE3314	MA 600	-494	0.3397, 0.3234, 0.3095	465	814	-29	-99	-107
JE3305	SHT	-200	0.2099, 0.2242, 0.2513	368	874	40	-17	-31
JE3306	SHT	-270	0.0883, 0.0894, 0.0816	438	893	43	-1	-10
6 m NaCl + 0.3 m KNO_3, 100°C (NO_3^-/Cl^- = 0.05) , pH 6.3								
JE3315	MA 600	-259	0.6496, 0.5996, 0.8536	278	402	-47	-84	-88
JE3316	MA 600	-533	0.7197, 0.704, 0.6882	211	315	-53	-78	-79
JE3307	SHT	-237	0.1971, 0.1721, 0.1951	140	420	5	-12	-14
JE3308	SHT	-243	0.2998, 0.2647, 0.2911	270	437	14	-5	-6
MA 600 = As received wrought specimens finished with paper 600 (polished), SHT = Solution heat-treated specimens containing the black annealed oxide film (BOF) on the surface (1121°C for 20 min plus water quenched). MH = Minor or no hysteresis								

TABLE 5
CHARACTERISTIC POTENTIALS (mV, SSC) AND CORROSION RATES FOR ALLOY 22

Specimen ID	Type of Specimen	E_{corr}, 24 h (mV, SSC)	Corrosion Rates (µm/year) After 24-h	E20 (mV, SSC)	E200 (mV, SSC)	ER10 (mV, SSC)	ER1 (mV, SSC)	ERCO (mV, SSC)
3.5 m NaCl + 0.525 m KNO_3, 60°C (NO_3^-/Cl^- = 0.15), pH 6.7								
DEA3383	MA 600	-293	0.1567, 0.08791, 0.1884	571	NA (A)	431	327	331 MH
DEA3384	MA 600	-170	0.5439, 0.557, 0.5548	NA (A)	NA (A)	440	288	364 MH
DEA3389	MA 600	-456	0.245, 0.295, 0.1557	(-128) AP, 596	854	629	336	808 MH
DEA3360	SHT	-81	0.1735, 0.1768, 0.1645	NA (A)	NA (A)	NA (A)	447	-18 MH
DEA3361	SHT	-186	0.7529, 0.7233, 0.7829	339	NA (A)	162	-78	-162 MH
3.5 m NaCl + 0.525 m KNO_3, 100°C (NO_3^-/Cl^- = 0.15), pH 6.7								
DEA3385	MA 600	-340	0.2588, 0.2467	448	NA (A)	80	-74	-32 / -82
DEA3386	MA 600	-207	1.398, 1.548, 1.377	337	NA (A)	177	-8	111 MH
DEA3390	MA 600	-480	0.292, 0.5749, 0.7618	(-90) AP 425	682	333	-5	-81
DEA3362	SHT	-257	0.9688, 0.9592, 0.8437	NA (A)	NA (A)	NA (A)	-71	-198 MH
DEA3363	SHT	-222	1.332, 1.284, 1.279	234	NA (A)	74	-69	-72
DEA3374	SHT	-316	1.291, 1.172, 1.527	742	930	76	-20	-2
0.1 m NaCl + 0.001 m $NaHCO_3$, 60°C (HCO_3^-/Cl^- = 0.01), pH 8.0								
DEA3377	MA 600	-472	0.158, 0.1184, 0.1071	735	857	381	263	400
DEA3379	MA 600	-413	0.1378, 0.1358, 0.107	(3) AP	NA (A)	NA (A)	458	NA
DEA3380	MA 600	NA	0.2295, 0.2397, 0.1542	NA (A)	NA (A)	NA (A)	420	NA
DEA3364	SHT	-252	0.2188, 0.2328, 0.2308	NA (A)	NA (A)	NA (A)	380	80 MH
DEA3365	SHT	-280	0.0319, 0.0392, 0.0363	NA (A)	NA (A)	NA (A)	497	126 MH
DEA3372	SHT	-206	0.0673, 0.0909, 0.0784	726	NA	746	538	NA
0.1 m NaCl + 0.001 m $NaHCO_3$, 95°C (HCO_3^-/Cl^- = 0.01), pH 8.0								
DEA3378	MA 600	-252	0.1558, 0.4024, 0.6637	329	771	32	-100	-141
DEA3381	MA 600	-267	0.3985, 0.1288, 0.4037	325	NA (A)	8	-105	-141
DEA3382	MA 600	-226	0.3275, 0.4018, 0.4753	331	NA (A)	57	-86	-129
DEA3366	SHT	-297	0.0377, 0.0990, 0.090	NA (A)	NA (A)	NA (A)	543	NA
DEA3367	SHT	-246	0.1673, 0.1673, 0.1867	536	NA (A)	255	92	-168 MH
DEA3373	SHT	-403	0.2191, 0.234, 0.227	195	319	116	-193	-278
MA 600 = As received wrought specimens finished with paper 600 (polished), SHT = Solution heat-treated specimens containing the black annealed oxide film (BOF) on the surface (1121°C for 20 min plus water quenched). MH = Minor or no hysteresis, (A) The maximum applied potential was +600 mV SSC, AP = Anodic Peak								

TABLE 6
OBSERVATIONS OF THE CREVICED SPECIMENS AFTER THE CPP TESTS

Solution	T (°C)	Specimens	**Observations**
1 M NaCl	60	MA 600	Yellow TP. Small dull CC
		SHT	Crystallographic CC. Some pitting corrosion in bold areas.
	90	MA 600	TP. Crystallographic CC. Caked corrosion products under CF.
		SHT	Crystallographic CC. No bold TP
5 M $CaCl_2$	60	MA 600	Small dull CC
		SHT	Isolated pitting-like attack, attack on edges following lamination directions. No CC
	90	MA 600	Typical Massive attack in bold surface, starting at the CF and following gravity, attack on edges.
		SHT	Edge attack following lamination directions, pitting-like attack, especially on corners. Stem edges attack.
6 m NaCl + 0.9 m KNO_3	80	MA 600	Bold TP. Dull, minimal CC. Some crystallographic CC
		SHT	Crystallographic CC. Some pitting corrosion on bold surfaces.
	100	MA 600	TP in bold surfaces. Dull and deep crystallographic CC.
		SHT	Crystallographic CC. Bold TP.
6 m NaCl + 0.3 m KNO_3	80	MA 600	Iridescent TP. Dull and Shiny Crystallographic CC
		SHT	Black Specimen. Crystallographic CC, deep at spots
	100	MA 600	TP. Deep crystallographic CC in almost every CF spot
		SHT	Black. Crystallographic CC in almost every CF spot.
3.5 m NaCl + 0.525 m KNO_3	60	MA 600	Shiny, little or no TP. No CC. No Localized Corrosion
		SHT	Black. No discoloration. Little or no CC. Edge attack.
	100	MA 600	Iridescent blue/tan TP. Small dull CC.
		SHT	Black. Small spotty CC. Some edge attack
0.1 m NaCl + 0.001 m $NaHCO_3$	60	MA 600	Bluish/Tan TP. No localized corrosion.
		SHT	Black. Blue discoloration. No localized corrosion. Attack on borders
	95	MA 600	Bluish/Tan TP. Small dull CC around the rim of CFs
		SHT	Black/Bluish. Little CC. Edge and border attack.
TP = Transpassivity, CC = Crevice Corrosion, CF = Crevice Former (total of 24 spots)			

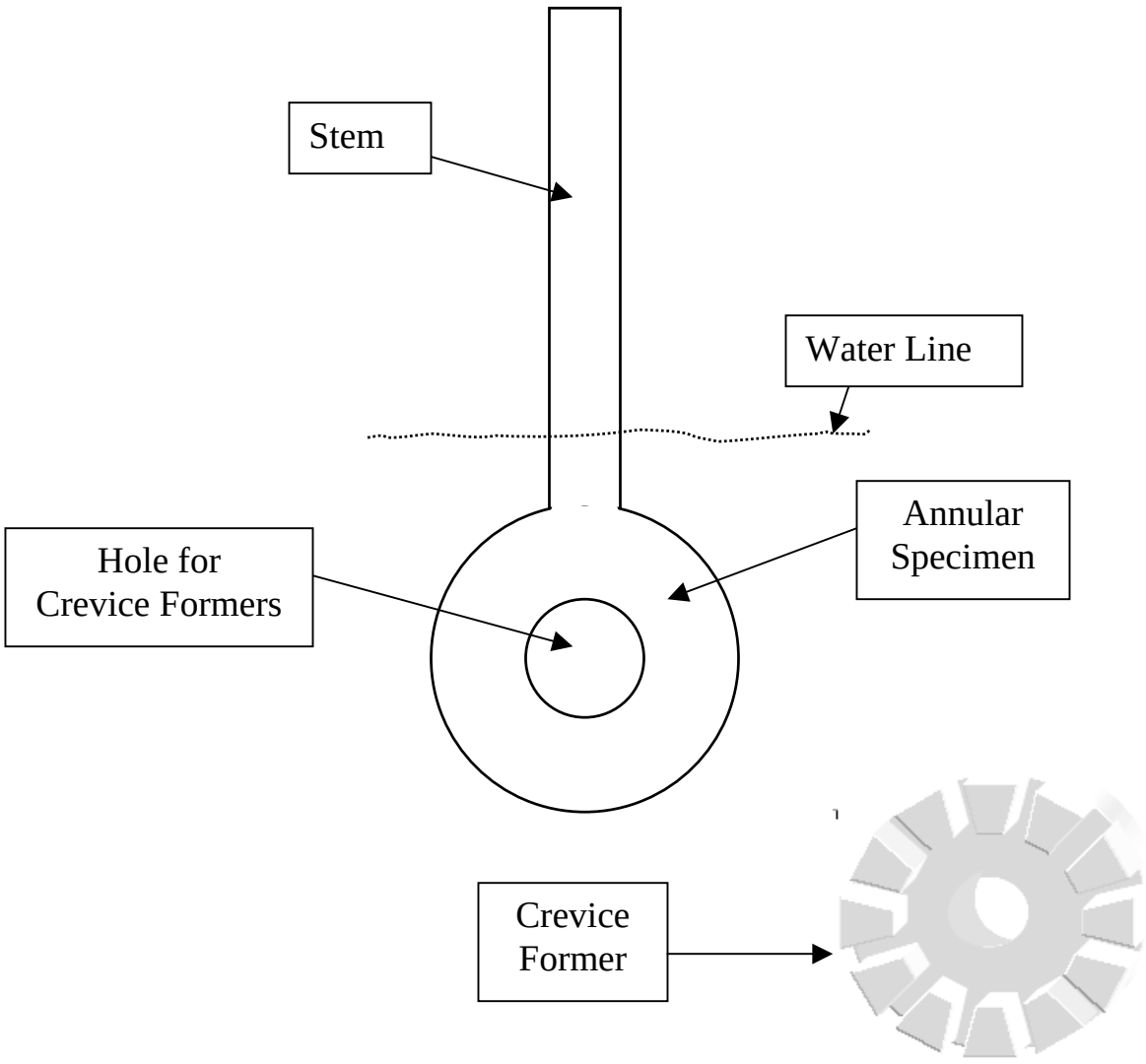

FIGURE 1 – Multiple Crevice Assembly (MCA) Specimen and Crevice Former (CF). Further photographs of the corroded specimens generally correspond to one quarter of the tested surface.

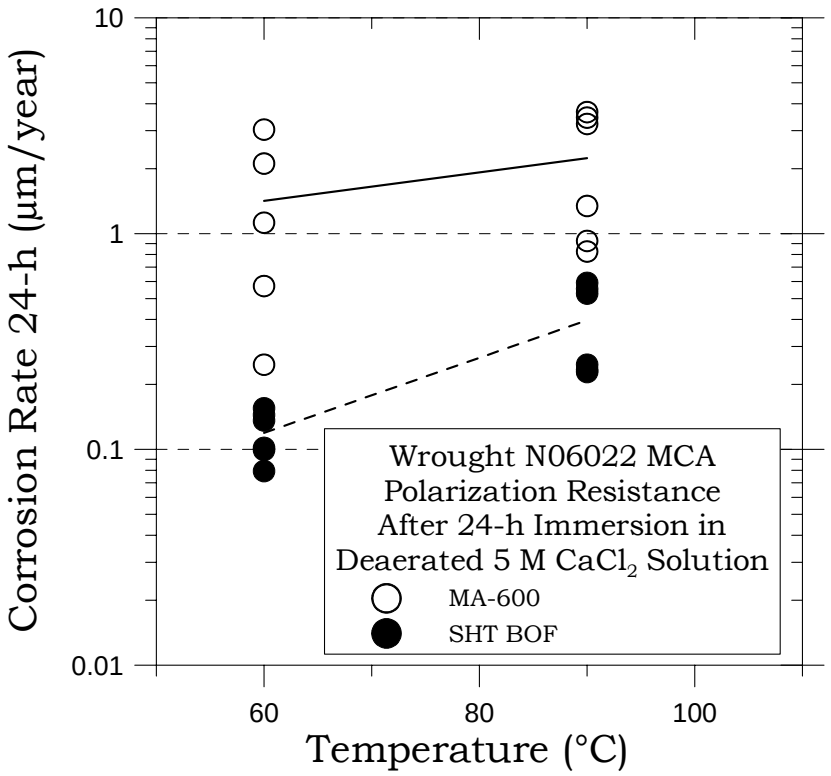

FIGURE 2 – CR for MA and SHT Alloy 22 Specimens in 5 M $CaCl_2$

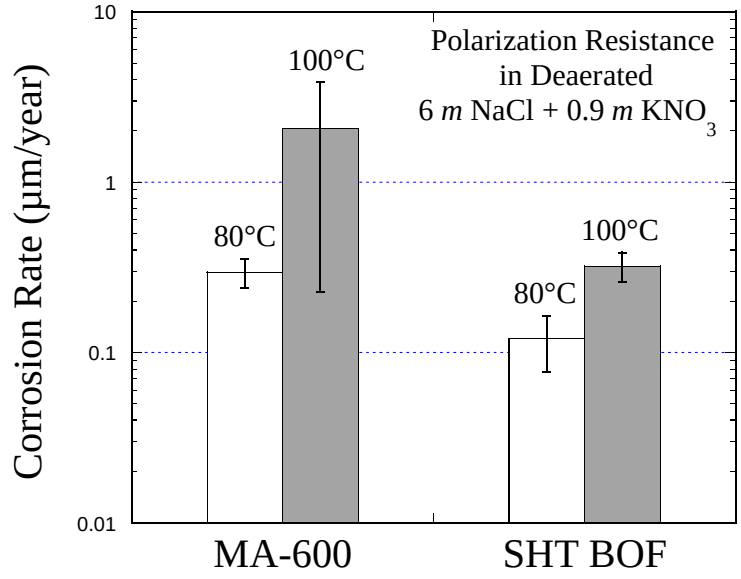

FIGURE 3 – CR for MA and SHT Alloy 22 Specimens in NaCl + KNO_3 Solutions

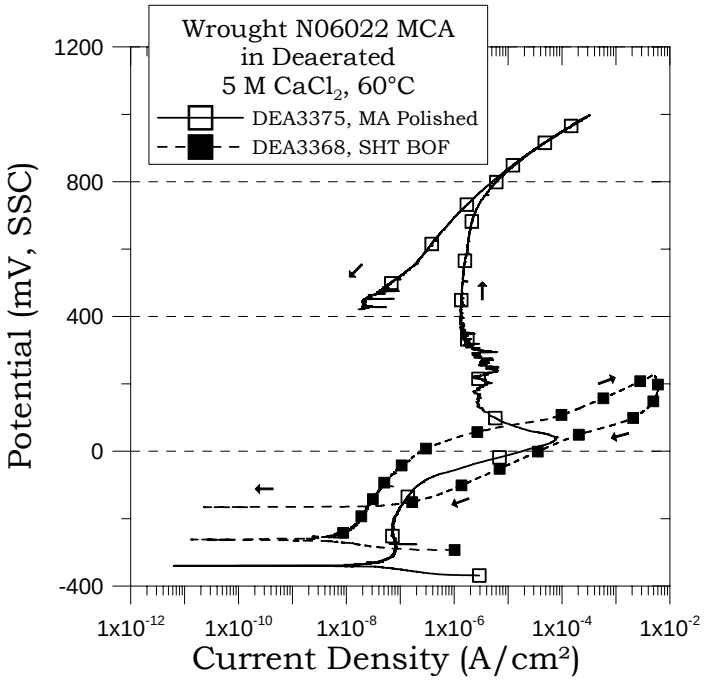

FIGURE 4 – Cyclic Potentiodynamic Polarization (CPP) for MA and SHT Alloy 22 Specimens in 5 M $CaCl_2$ at 60°C

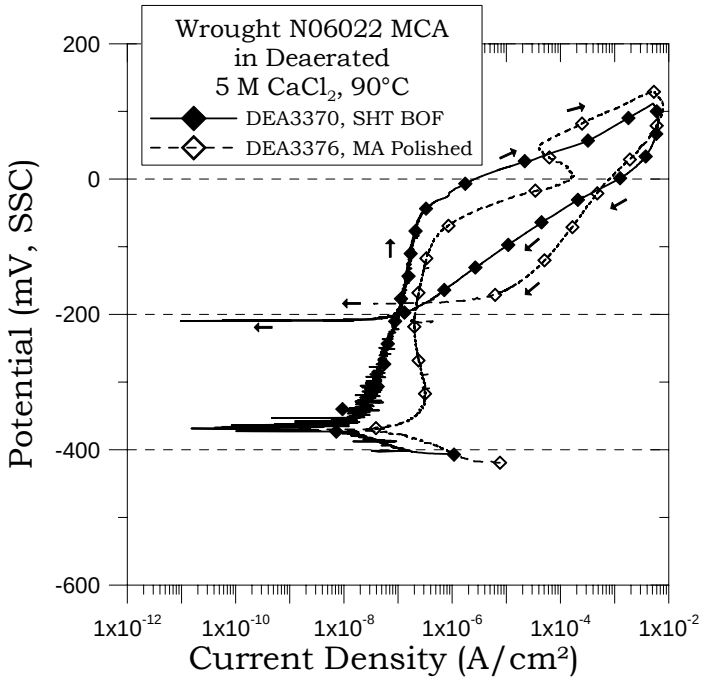

FIGURE 5 – CPP for MA and SHT Alloy 22 Specimens in 5 M $CaCl_2$ at 90°C

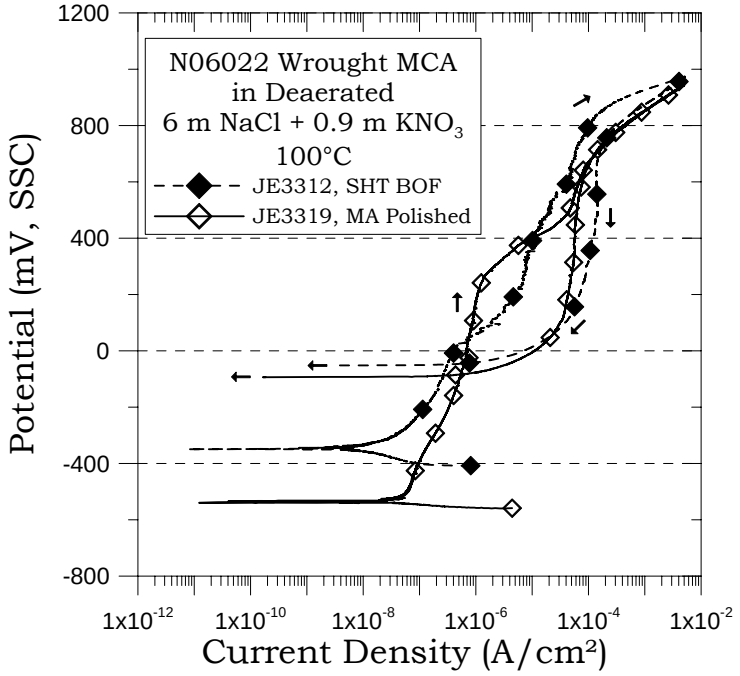

FIGURE 6 – CPP for MA and SHT Alloy 22 Specimens in 6 m NaCl + 0.9 m KNO_3 at 100°C

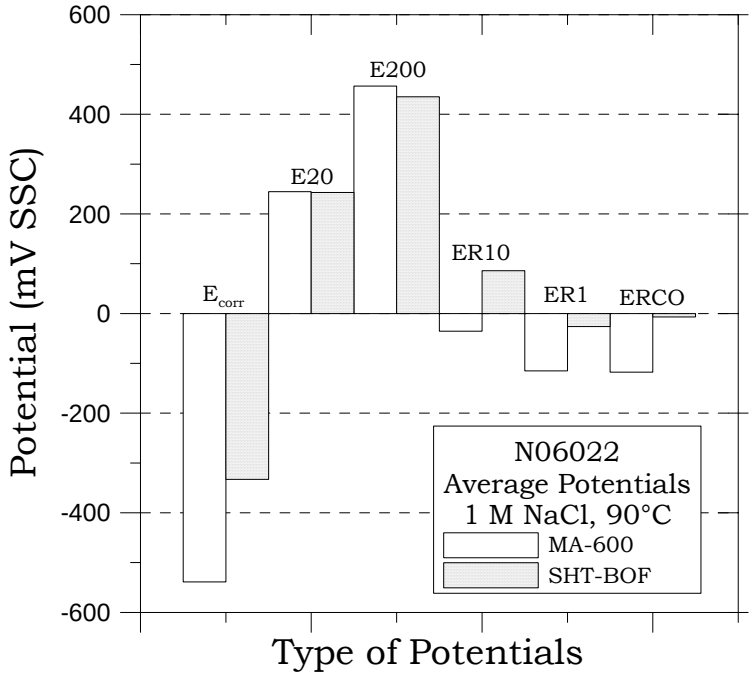

FIGURE 7 – Parameters from CPP for MA and SHT Alloy 22 in 1 M NaCl at 90°C

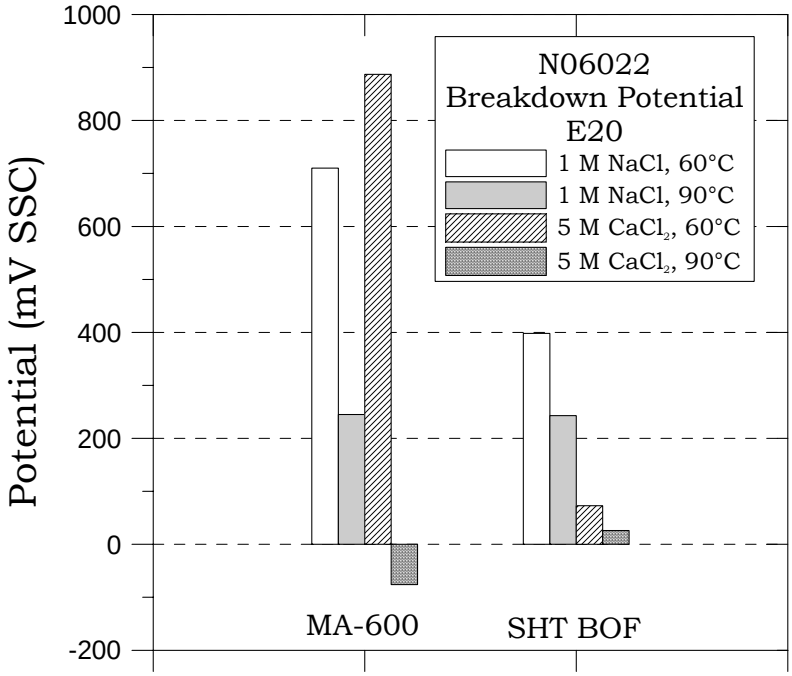

FIGURE 8 – Average Breakdown Potential E20 for MA and SHT Alloy 22 Specimens in 1 M NaCl and 5 M $CaCl_2$

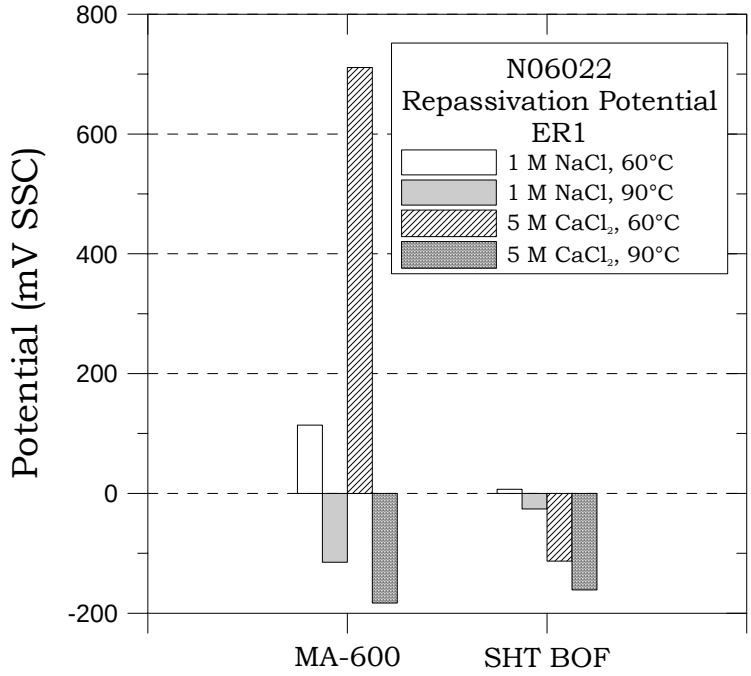

FIGURE 9 – Average Repassivation Potential ER1 for MA and SHT Alloy 22 Specimens in 1 M NaCl and 5 M $CaCl_2$

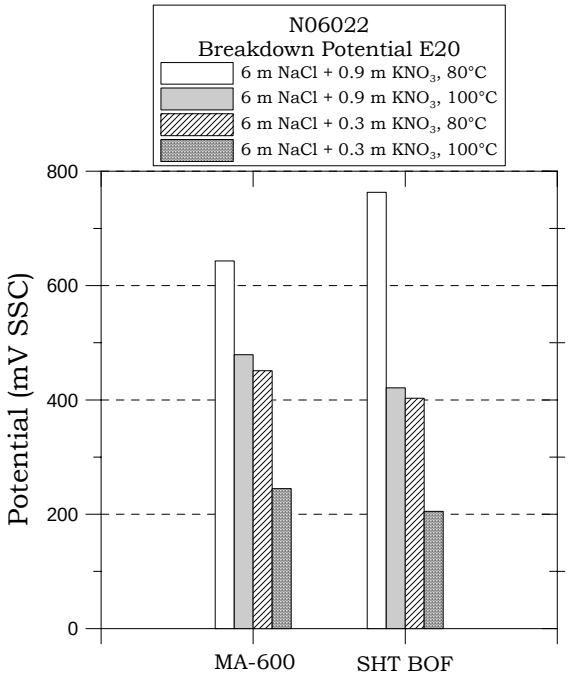

FIGURE 10 – Average Breakdown Potential E20 for MA and SHT Alloy 22 Specimens in 6 m NaCl solutions

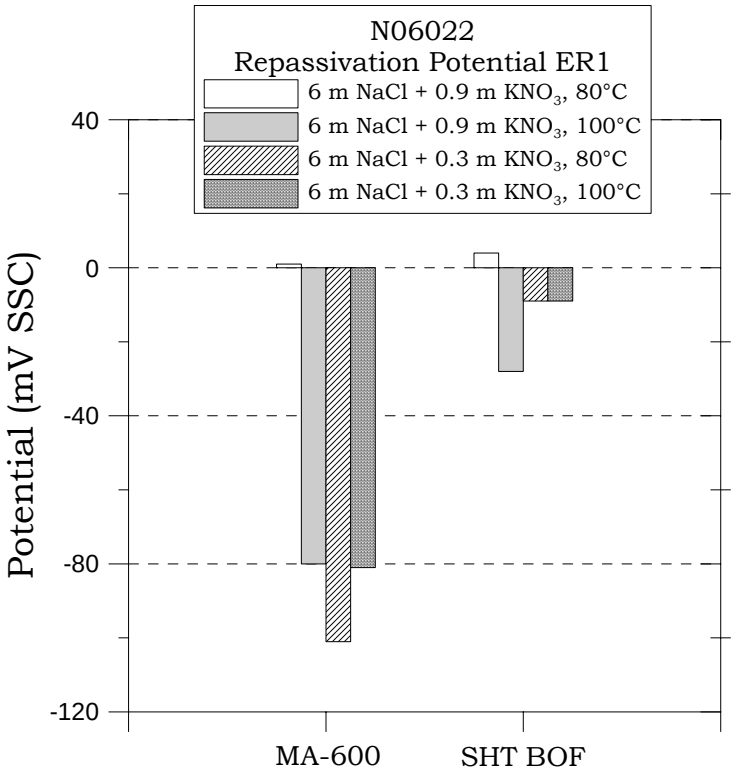

FIGURE 11 – Average Repassivation Potential ER1 for MA and SHT Alloy 22 Specimens in 6 m NaCl solutions

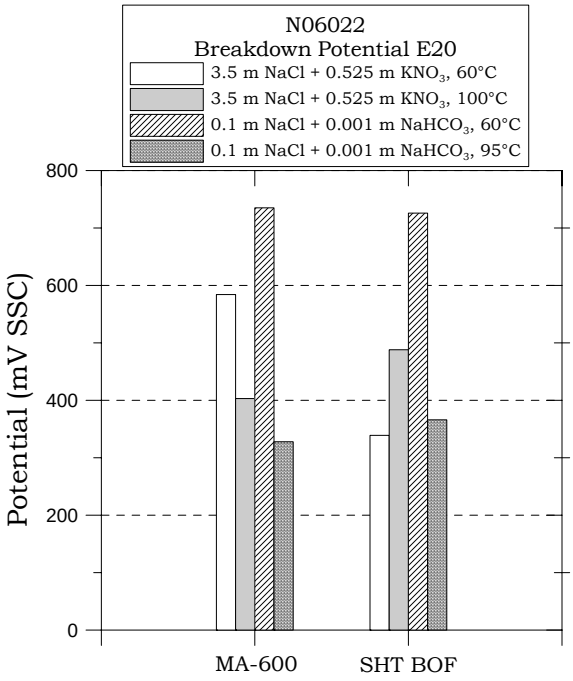

FIGURE 12 – Average Breakdown Potential E20 for MA and SHT Alloy 22 Specimens in 3.5 m NaCl + 0.525 m KNO_3 and 0.1 m NaCl + 0.001 m $NaHCO_3$

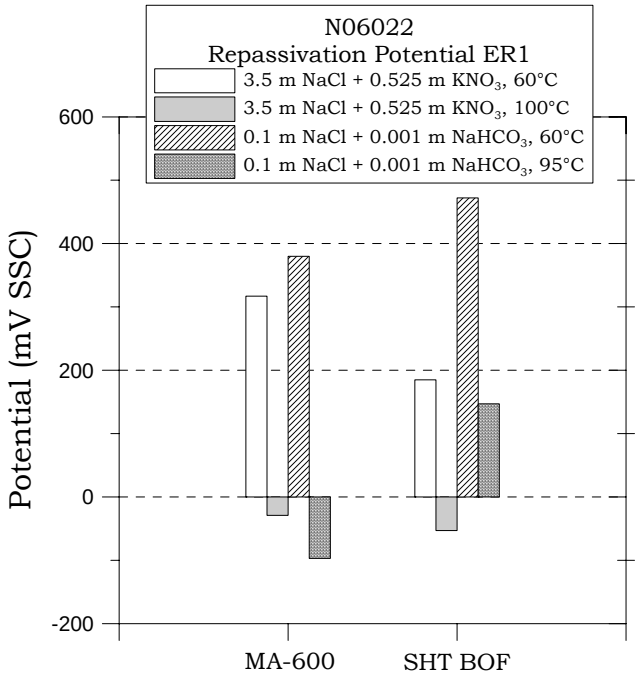

FIGURE 13 – Average Repassivation Potential ER1 for MA and SHT Alloy 22 Specimens in 3.5 m NaCl + 0.525 m KNO_3 and 0.1 m NaCl + 0.001 m $NaHCO_3$

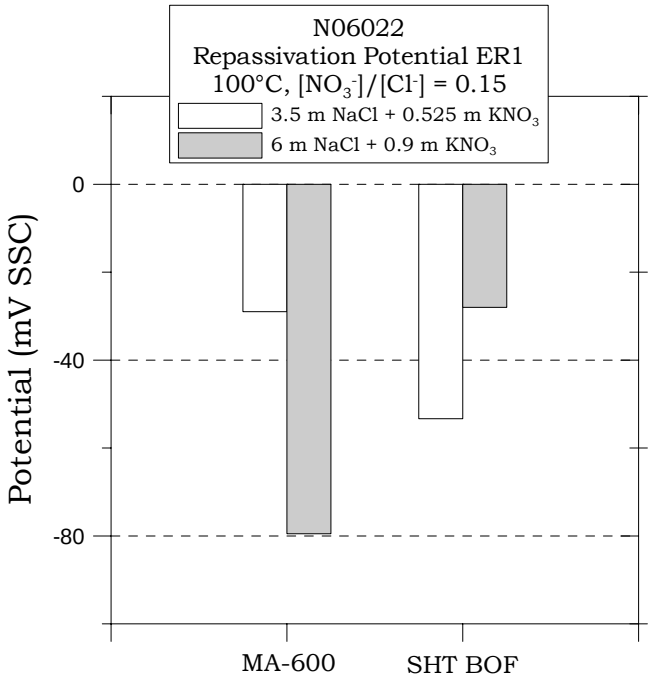

FIGURE 14 – Average Repassivation Potential ER1 for MA and SHT Alloy 22 Specimens in NaCl + KNO_3 solutions at 100°C

FIGURE 15 – Specimen JE3328, MA polished Alloy 22 after CPP in 1 M NaCl at 90ºC

FIGURE 16 – Specimen JE3303, SHT Alloy 22 after CPP in 1 M NaCl at 90ºC

FIGURE 17 – Specimen JE3315, MA Alloy 22 after CPP in 6 m NaCl + 0.3 m KNO_3 at 100ºC

FIGURE 18 – Specimen JE3308, SHT Alloy 22 after CPP in 6 m NaCl + 0.3 m KNO_3 at 100ºC

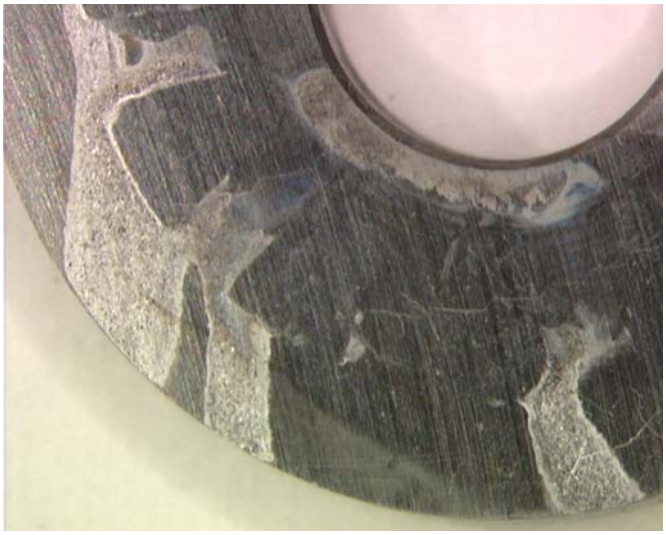

FIGURE 19 – Specimen JE3376, MA polished Alloy 22 after CPP in 5 M $CaCl_2$ at 90ºC

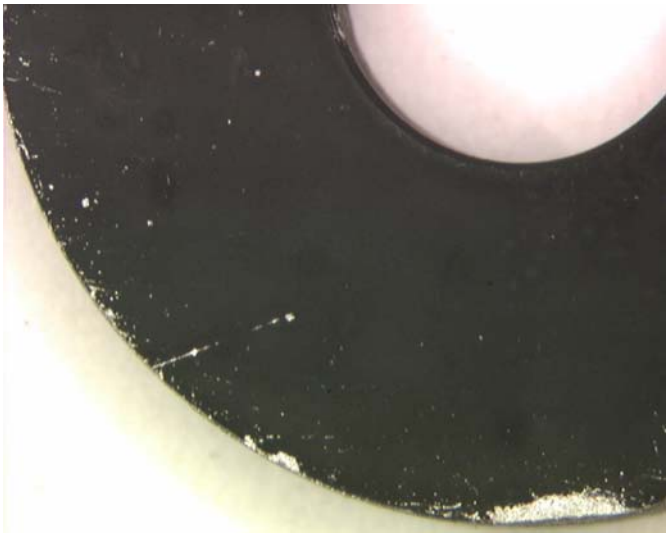

FIGURE 20 – Specimen JE3370, SHT Alloy 22 after CPP in 5 M CaCl2 at 90ºC

FIGURE 21 – Specimen JE3381, MA polished Alloy 22 after CPP in 0.1 m NaCl + 0.001 m $NaHCO_3$ at 95ºC

FIGURE 22 – Specimen JE3373, SHT Alloy 22 after CPP in 0.1 m NaCl + 0.001 m $NaHCO_3$ at 95ºC

FIGURE 23 – Specimen JE3380, MA polished Alloy 22 after CPP in 0.1 m NaCl + 0.001 m $NaHCO_3$ at 60ºC

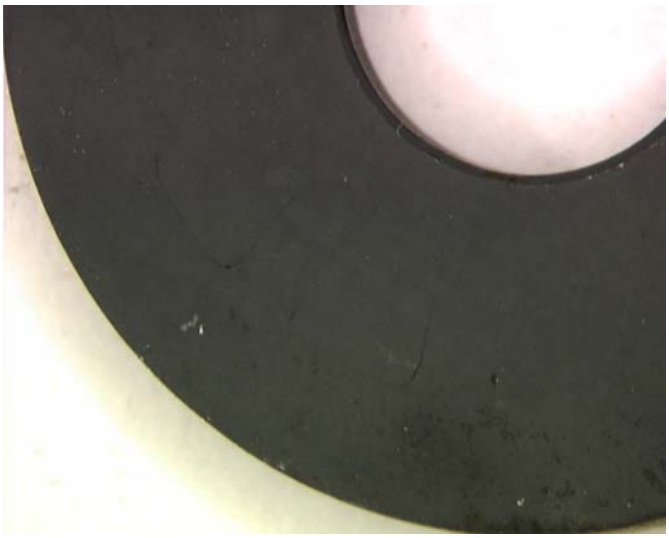

FIGURE 24 – Specimen JE3372, SHT Alloy 22 after CPP in 0.1 m NaCl + 0.001 m $NaHCO_3$ at 60ºC